

Crystallisation of amorphous Al-Sm-Ni-(Cu) alloys.

F.G. Cuevas¹, S. Lozano-Perez², R.M. Aranda¹, E.S. Caballero³

¹ Department of Chemical Engineering, Physical Chemistry and Materials Science, Escuela Técnica Superior de Ingeniería, University of Huelva, Campus El Carmen, Avda. Tres de marzo s/n, 21071 Huelva, Spain

² Department of Materials, University de Oxford, 16 Parks Road, Oxford OX1 3PH, UK

³ Department of Materials Science and Engineering, Escuela Técnica Superior de Ingeniería, University of Sevilla, Camino de los Descubrimientos s/n, 41092 Sevilla, Spain

Correspondence: F.G. Cuevas, fgcuevas@dqcm.uhu.es

Abstract.

The primary crystallisation and intermetallics formation of an amorphous Al₈₈-Sm₄-Ni₈ alloy has been studied. The effect of 1 at% Cu substituting Al or Ni is also considered. The initial microstructure of the melt-spun ribbons is studied by X-ray diffraction. Differential scanning calorimetry shows that the thermal stability of the amorphous alloy is affected by Cu, increasing when Cu substitutes Al and decreasing when substituting Ni. Transmission electron microscopy shows that Cu reduces the size of the initial nanocrystals. After the high-temperature stages of crystallisation, the developed structure is analysed in detail by combining X-rays diffraction, differential scanning calorimetry and transmission electron microscopy. The study includes the effect of Cu on the appearance sequence and characteristics of the intermetallics up to 600 °C. Cu retards the appearance of the stable Al₁₉Sm₃Ni₅ phase, with an acicular shape being more easily developed.

Keywords: amorphous metals; Al-Sm-Ni alloys; nucleation and growth; rapid solidification; microstructure; high-temperature crystallization

1. Introduction.

Amorphous aluminium-rich alloys have been intensively studied during the last 30 years because of their greater strengths with respect to conventional

aluminium alloys and great potential for practical applications [1]. For some alloys, the strength can be further increased by partial crystallisation of the amorphous phase to form a fine distribution of α -Al nanocrystals [2]. In the systems Al-RE-Ni (RE = rare earth), ultimate tensile strength values of 1100 and 1560 MPa [3, 4] have been respectively reported for the amorphous and partially crystalline alloys, resulting to be higher than those obtained in crystalline aluminium alloys.

The strengthening mechanism promoting these high figures after nanocrystallisation can be explained by the increase in the resistance to shear slip caused by the homogeneous distribution of primary α -Al nanocrystals [3]. Also, the higher strength due to solute enrichment of the remaining amorphous matrix can explain the attained values [5]. Both factors have also been considered to act together [6]. Independently of the cause, the number density, size and distribution of nanocrystals, which depend on the alloy composition and crystallisation procedure, seem to be a key factor on the properties of nanocrystallised materials [6]. In this line, Cu addition has been proved to reduce the size of α -Al nanocrystals [7], improving mechanical properties after primary crystallisation.

Amongst the different possible systems to study, each one with different properties, the system Al-Sm-Ni is of interest because of the very wide glass forming range of the Al-Sm binary alloys, the widest among Al-RE alloys [8]. In this work, the effect of Cu on the primary crystallisation of the alloy $\text{Al}_{88}\text{-Sm}_4\text{-Ni}_8$ is evaluated. Moreover, a detailed study of the effect of Cu on high temperature crystallisation is carried out, a stage of crystallisation still nowadays not totally well described. Despite intermetallics formation lowers mechanical properties, information on the thermal stability and mechanisms of decomposition at high temperatures is of great interest to approach the properties obtained after consolidation into bulk materials. Actual processes of consolidation for these compositions usually result in the presence of some intermetallics [9, 10], thus the interest in these high temperatures processes.

2. Experimental procedure.

The $\text{Al}_{88}\text{-Sm}_4\text{-Ni}_8$ alloy, and the substitution of Cu for Al or Ni, resulting in the compositions $\text{Al}_{87}\text{-Sm}_4\text{-Ni}_8\text{-Cu}_1$ or $\text{Al}_{88}\text{-Sm}_4\text{-Ni}_7\text{-Cu}_1$, have been studied.

Metals with high purity (Al 99.9%, Ni 99.95%, Sm 99.9% and Cu 99.9%) were vacuum arc melted after Ti-gettering to obtain the master alloys Al₉₀-Cu₁₀ and Al₂₅-Sm₇₅ with melting temperature of 600 °C and 740 °C respectively. Master alloys and additional pure metals to balance the desired final composition were arc melted a second time. The amorphous alloys were obtained in form of ribbons (25 – 30 µm thick and 1 –2 mm wide) by melt spinning the alloy after heating at 1000 °C in a 200 mbar He atmosphere. The wheel speed was 40 m/s and the distance nozzle-wheel 1.5 mm.

X-rays diffraction (XRD) and transmission electron microscopy (TEM) were used to examine the microstructure of the melt-spun and heat treated ribbons. Heat treatments were carried out in a differential scanning calorimeter (DSC), also used to examine the thermal stability of the materials from room temperature to 600 °C.

XRD studies were carried out in a Philips PW 1729 using a Cu-K_α radiation for 2θ between 20 and 80°, step size of 0.02° and scan speed of 0.02 °/s. For TEM studies, a Philips CM20 microscope operating at 200 KV was used. Specimens were prepared by electropolishing in a solution of 10 % perchloric acid in 90 % ethanol, at -30 °C approximately. In some cases, this was followed by ion beam milling process after cooling the specimens for 0.5 hours at -30 °C. For DSC studies, a TA Instruments 2010, heating at 20 °C/min under a protective Ar atmosphere, was used.

A detailed examination of the chemical composition was carried out by means of scanning transmission electron microscopy (STEM, VG HB501 at 100 kV) after high temperature crystallisation.

3. Result and discussion.

3.1. Melt-spun ribbons

XRD patterns of the melt-spun ribbons for the three studied compositions are shown in Figure 1. A broad and small peak, distinctive of amorphous structures, can be observed in the three patterns. Areas of short range local order, sometimes found in form of a small shoulder in the broad peak in other Al-RE-Ni systems, are not found in the studied materials. The high atomic radius difference between Al and Sm results in a high glass forming

ability according to the confusion principle [11]. It is therefore possible to state that ribbons prepared in this work are amorphous, at least at an XRD analysis.

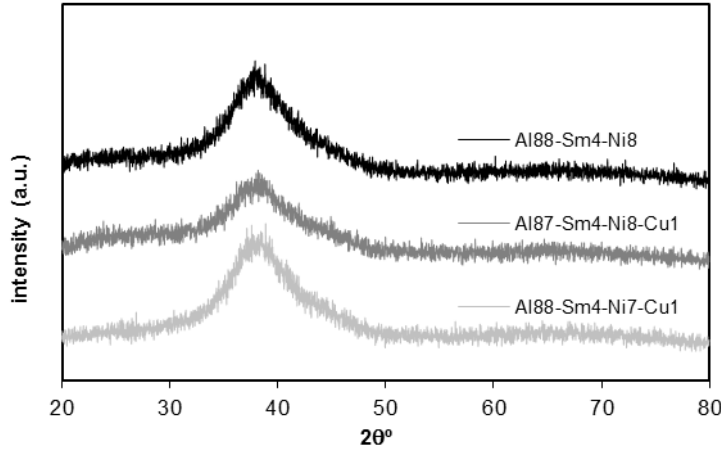


Figure 1. XRD patterns of melt-spun ribbons of the studied alloys.

This same behaviour is described several times in the literature [12-15] for the same or similar compositions. Nevertheless, a slightly different behaviour, with quenched-in nanocrystals in melt-spun ribbons, only visible under high resolution TEM, has also been reported [16], or even clearly nanocrystalline [17] or crystalline structures [18]. The melt spinning parameters must be the reason for these differences.

3.2. Crystallisation process

DSC traces of melt-spun ribbons are shown in Figure 2. Three main stages or reactions are observed during the crystallisation process, although a fourth small exothermic reaction is also present, more clearly seen for the Cu-free alloy.

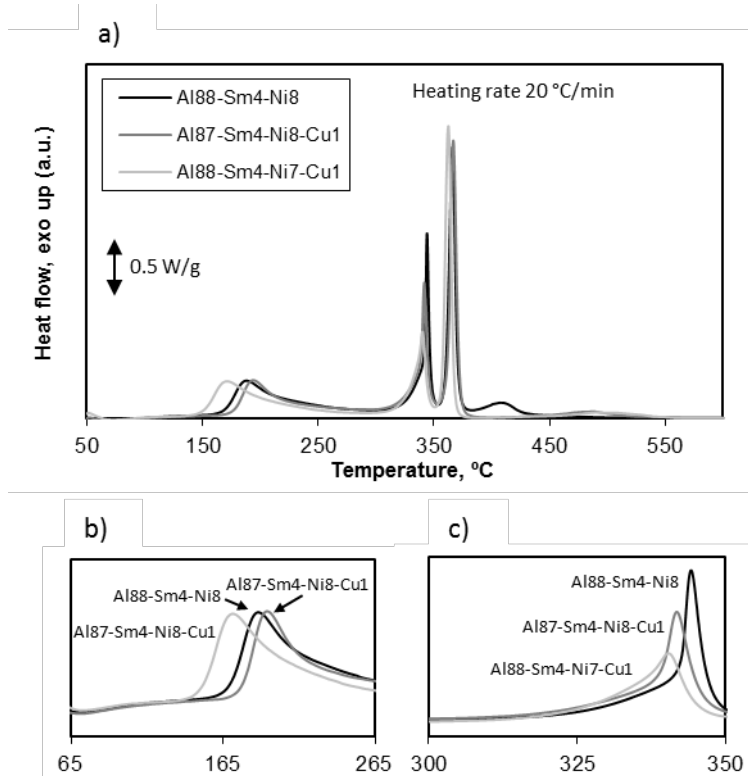


Figure 2. a) DSC traces of melt-spun ribbons of the studied alloys, and details of b) the first and c) the second crystallisation reactions.

The observed four reactions in DSC traces are usually found in alloys of similar compositions [7, 13, 15, 18-20], although the intensity and precise position of the reactions depends on composition [17] and heating rate [19, 21]. Also, only the first three reactions are sometimes reported [7, 14, 16, 17, 21, 22], although up to five reactions have been identified [23]. Again, composition and heating rate affect these differences.

In general, this is a usual behaviour in Al-RE-Ni alloys with Y, Sm, Ce, Nd, La, etc., where the primary crystallisation causes the appearance of α -Al nanocrystal (or also intermetallics for high solute contents). The high temperature reactions are due to the crystallisation of the remaining amorphous matrix, inducing the precipitation and transformation of diverse intermetallics.

3.3. Primary crystallisation

Primary crystallisation is related to a broad DSC reaction with an onset temperature at 160 °C and a maximum at 188 °C for the Cu-free alloy. According to the area under the DSC curve, this reaction represent a 35% of

the total energy of crystallization for the Cu-free alloy. This primary crystallization also shows a pre-reaction from approximately 70 °C (Figure 2b). Considering that nucleation should not be observed before the onset temperature of the reaction, this pre-reaction can be related to the growth of pre-existing nanocrystals in the as-spun state, and/or to structural relaxation phenomena of the amorphous phase.

As shown in Figure 3 for ribbons treated to 250 °C, i.e., once the first reaction has finished and far of the next one, XRD demonstrate that this first reaction is related to the appearance of α -Al nanocrystals. The process takes place by nucleation and growth from totally amorphous structures [10, 24, 25], although could just be a growth process for ribbons with quenched-in nanocrystals. Evidence of remaining amorphous phase in diffraction patterns is hardly observed after heating to 250 °C, when the nucleation and growth processes of α -Al nanocrystals must be almost completed. Just a certain curvature in the XRD background can be found near the main Al peak. Note that the volume fraction transformed to α -Al could be higher than the aforementioned 35% for the Cu-free alloy, if Al crystals partially intervene in the subsequent crystallization processes.

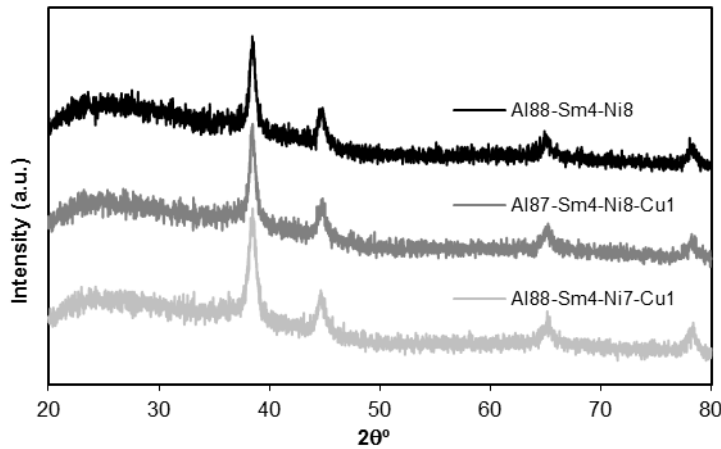


Figure 3. XRD patterns of heat treated ribbons to the end of the first DSC crystallisation stage (250 °C). Observed peaks correspond to α -Al nanocrystals.

On the other hand, the absence of intermetallic phases during primary crystallisation can be explained because refused solute atoms must easily diffuse and do not accumulate around Al nanocrystals [26].

Crystallisation is affected by the presence of Cu in the alloys. When 1 at% Al is replaced by Cu, the reaction is slightly shifted to higher temperatures (Figure 2b), with onset temperature at 165 °C and maximum at 195 °C, and the reaction representing a 32% of the total energy of crystallization. The total amount of solute increases, resulting in a more stable amorphous structure. When 1 at% Ni is replaced by Cu, the amount of solute does not vary, but the atomic radius difference for Al-Cu is smaller than that of Al-Ni. The higher similarity among the components could account for the stability reduction of this amorphous alloy. The reaction is shifted to a lower onset temperature of 140 °C, with the maximum at 170 °C, and being a 38% of the whole crystallization process energy.

The lattice parameter of the α -Al crystals, measured from the peaks position in XRD patterns of Figure 3, is 0.4043 ± 0.0004 nm for the Cu-free and 0.4048 ± 0.0002 nm for both Cu-containing alloys. These values, smaller than that of pure Al, 0.4050 nm, indicate the presence of alloying elements in the solid solution. In particular, Ni with a radius of 0.1246 nm (vs. 0.1432 and 0.1802 nm for Al and Sm respectively) must play an important role in the solid solution. This is however not always the reported behaviour. E.g., a value of 0.4061 nm was measured after primary crystallisation in an Al₈₈-Sm₆-Ni₆ alloy [13].

Nanocrystals size measurement was carried out on TEM micrographs. It was studied the situation after heating further the first DSC reaction, i.e., at 250 °C, the situation also studied in Figure 3, and with a similar volume fraction of nanocrystals of 35, 32 and 38 % according to the area under DSC curves of the three studied alloys. Results show that Cu reduces nanocrystals size by approximately 15 %, from 10.7 nm for the Cu-free alloy to about 9 nm for both Cu-containing alloys (Figure 4). Reduced diffusion and increased atomic bonding strength due to Cu segregation around Al nuclei could contribute to growth limitation, increasing the number of nanocrystals. Also, heterogeneous nucleation at Cu clusters or reduction of the nucleation barrier for α -Al nanocrystals could be considered, in this case directly increasing the number of nanocrystals. The actual situation is not clear, the reduction of the nucleation barrier has been proposed in other alloys as Al-Y-Ni-Cu [27] and Al-Ce-Ni-Cu [28], however, Cu has been reported both to be uniformly distributed in these alloys [7], and also to provoke compositional fluctuations [28, 29].

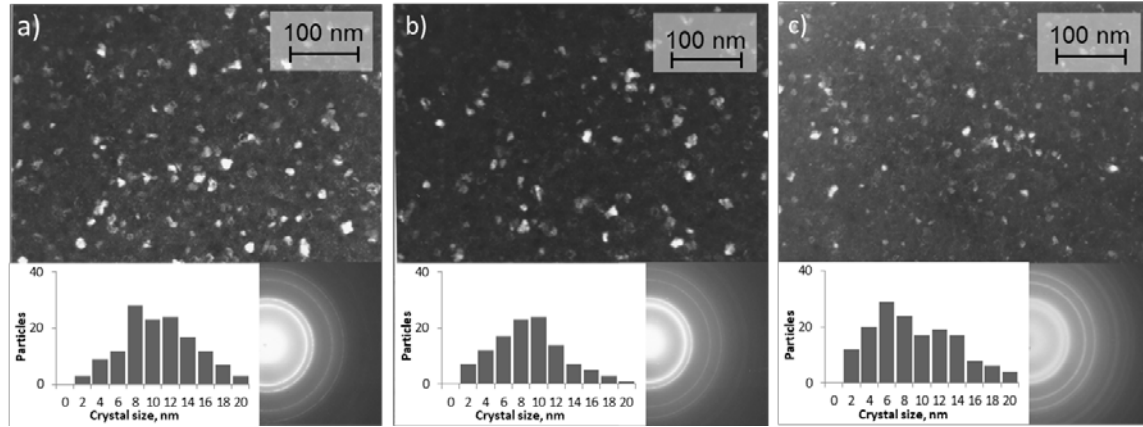


Figure 4. TEM dark field images and diffraction patterns of ribbons heat treated to the maximum temperature of the first DSC reaction of a) $\text{Al}_{88}\text{-Sm}_4\text{-Ni}_8$, b) $\text{Al}_{87}\text{-Sm}_4\text{-Ni}_8\text{-Cu}_1$ and c) $\text{Al}_{88}\text{-Sm}_4\text{-Ni}_7\text{-Cu}_1$ alloys. Nanocrystals counts are also shown.

As shown in Figure 4, the observed shape of the nanocrystals is in general rounded, as reported in [7, 23], although some dendritic-like shapes seem to be appearing, as reported in [24]. Whichever the shape, according to Figure 3 and TEM diffraction patterns of Figure 4, only α -Al nanocrystals were measured.

3.4. Second crystallisation stage

The second exothermic reaction in Figure 2 (detailed in Figure 2c), with an onset temperature approximately at 320 °C, represents the 23, 24 and 20% of the total energy of crystallization for the Cu-free and the two Cu-containing alloys, respectively. This reaction takes place at a smaller range of temperatures than the first one, with the third reaction almost starting before the second one has totally finished. A higher separation, desirable for the study of this reaction, is attained by heating the ribbons at 20 °C/min up to 5 °C before the onset of the second reaction, followed by an isothermal heat treatment. Figure 5 shows the new DSC traces, where the second reaction appears divided into two different ones, more clearly for the Cu-free alloy. The third reaction remains as only one, starting after 5-10 min of the second one, and apparently being easier for the Cu-free alloy.

A detailed examination of the DSC traces in Figure 2c (heating at 20 °C/min) shows that the second reaction has a tail at the low temperatures side, which appears as a different reaction during isothermal heat treatments.

In addition, the Cu-free alloy shows a bigger second subreaction, more clearly differentiated in the isothermal treatments.

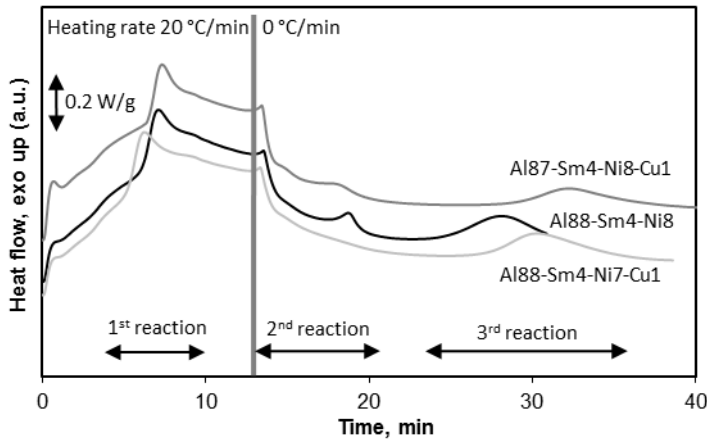


Figure 5. DSC traces carried out at 20 °C/min up to 5 °C before the onset of the second reaction, continuing with an isothermal heat treatment. The vertical line in the graph separates both heating regimes.

TEM micrographs acquired after heating to the end of the second reaction (i.e., at 20 °C/min up to 5 °C before the onset of the second reaction followed by 10 min of isothermal treatment) reveal a microstructure very similar to that observed after the first DSC reaction (Figure 6). In XRD patterns, also shown in Figure 6, only α -Al nanocrystals can surprisingly be identified. This is in agreement with previously reported results [21, 22], although the presence of unidentified intermetallics has also been suggested [20-22]. The second crystallisation reaction has also been associated with the formation of Al_3Sm (cubic + hexagonal) and an unknown metastable phase [17, 19], or with Al_3Ni and Al_3Sm [23]. Moreover, the study [13] of the onset and peak temperatures of the second DSC reaction in alloys with different compositions, and the null effect of varying the Ni content for a fixed amount of Sm, suggested the appearance of Al-Sm intermetallics, in particular orthorhombic $\text{Al}_{11}\text{Sm}_3$. Differences in the aforementioned results might be due to changes of chemical compositions and thermal treatments in the studied alloys.

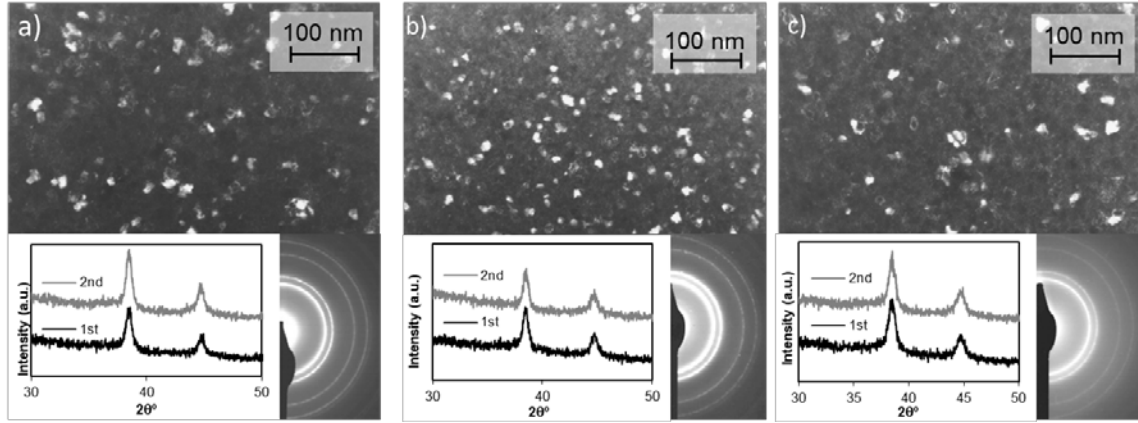


Figure 6. TEM dark field images and diffraction patterns of heat treated ribbons up to the end of the second DSC reaction of a) $\text{Al}_{88}\text{-Sm}_4\text{-Ni}_8$, b) $\text{Al}_{87}\text{-Sm}_4\text{-Ni}_8\text{-Cu}_1$ and c) $\text{Al}_{88}\text{-Sm}_4\text{-Ni}_7\text{-Cu}_1$ alloys. XRD patterns (both after the end of the first and second subreaction, i.e., after 3 and 10 min of isothermal heating) are also shown.

In the present work, on the bases of XRD and TEM results, it is not possible to identify any other phase than $\alpha\text{-Al}$ after the second DSC reaction. Nevertheless, new phases should be nucleating to an extent. Although it is not easy to confirm their existence, a very small asymmetry in the left side of the main Al peak suggests they might be present. According to the aforementioned studies, probably the nucleation of both Al_3Ni and Al-Sm or Al-Sm-Ni intermetallics, together with $\alpha\text{-Al}$ grains growth, could be a plausible explanation for this reaction.

The probable nucleation of these new phases around pre-existing $\alpha\text{-Al}$ nanocrystals surely hinders their identification after the nucleation process. A simple calculation can be carried out by assuming that the activation energy for the formation of intermetallic phases can be a 25% higher than that of $\alpha\text{-Al}$ nanocrystals [26], and also that, for instance for the Cu-free alloy, the crystallization energies from the DSC curves represent the aforementioned values of 35 and 23% for the first and second reaction. Moreover, considering that $\alpha\text{-Al}$ nuclei about 10.7 nm in diameter (640 nm^3) have formed in the first DSC reaction, and assuming a similar number density of intermetallics, particles of 8.45 nm in diameter should be formed in case of homogeneous nucleation and growth of the new intermetallics. However, a layer of 1.5 nm should be growing around existing $\alpha\text{-Al}$ nanocrystals. Despite the uncertainties in the previous reasoning, isolated particles should be easier to detect by XRD than very thin layers around

nanocrystals, therefore the heterogeneous nucleation around existing α -Al nanocrystals being more probable. Nevertheless, the appearance of these intermetallics needs to be corroborated with the study of the subsequent reactions.

3.5. Third/Fourth crystallisation stage

After heat treatments at temperatures beyond the second DSC reaction, intermetallics can be clearly identified, as shown by XRD after heating at 20 °C/min to selected temperatures (Figure 7). These heat treatments, chosen to show the intermetallics evolution, were carried out to the maximum of the third DSC reaction at about 365 °C, to the end of the third DSC reaction at 375 °C plus 30 min at this temperature (375 °C + 30'), to 450 °C and to 600 °C.

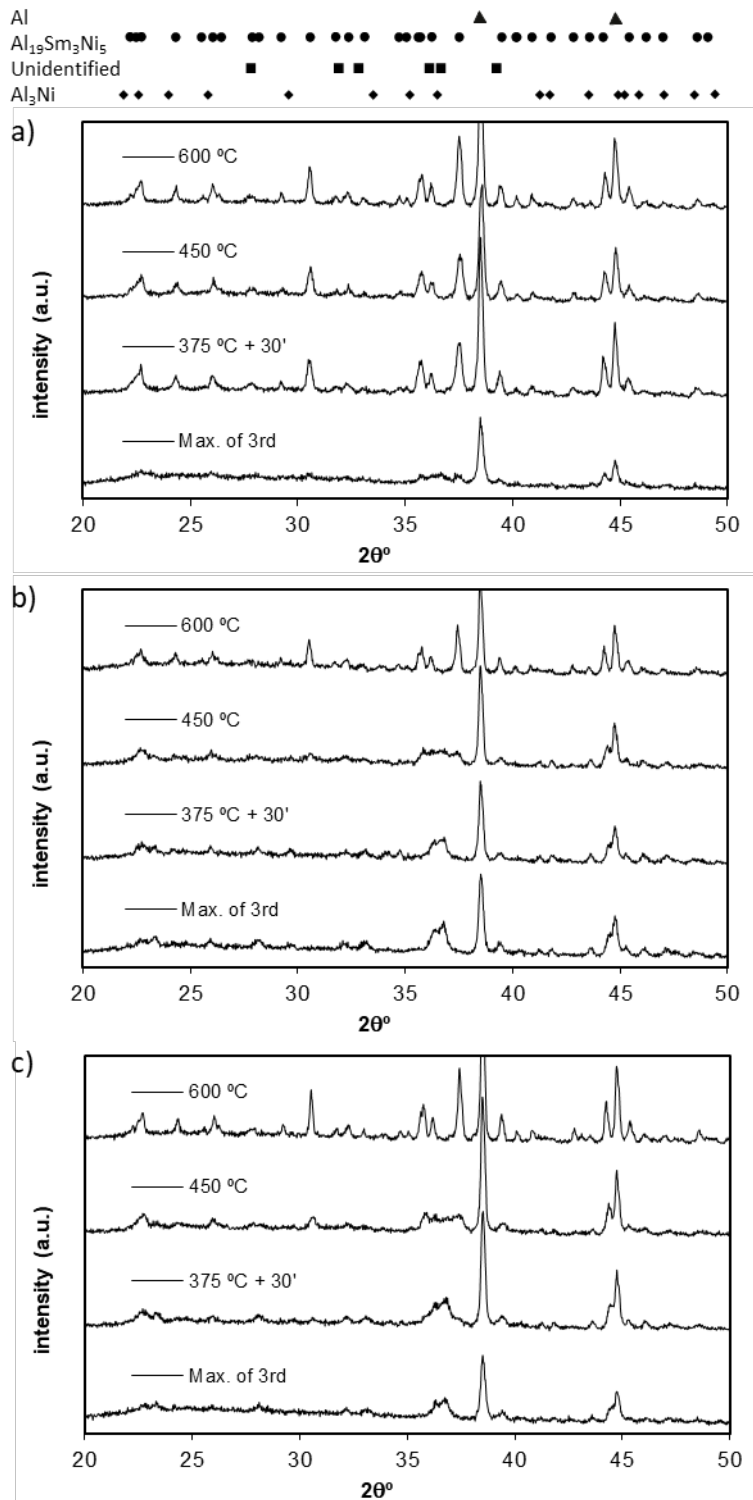


Figure 7. XRD patterns of a) $\text{Al}_{88}\text{-Sm}_4\text{-Ni}_8$, b) $\text{Al}_{87}\text{-Sm}_4\text{-Ni}_8\text{-Cu}_1$ and c) $\text{Al}_{88}\text{-Sm}_4\text{-Ni}_7\text{-Cu}_1$ heat treated ribbons at 20 °C/min to the temperature of the maximum of the third DSC reaction, to 375 °C + 30', to 450 °C and to 600 °C.

A detailed examination of the peaks positions and intensities needs to be carried out to identify the phases present in Figure 7. After heating to the maximum of the third DSC reaction at about 365 °C, Al and very probably a small amount of Al_3Ni are present for the three compositions studied. Moreover, an unidentified metastable phase appears (note for instance the double peak at about 36-37°), much more clearly seen if Cu is added to the alloy, whereas an additional small amount of a stable phase (note for instance the three peaks between 35 and 38°) seem to be present in the Cu-free alloy. The prevalence of the metastable phase is therefore favoured by the addition of Cu.

Results after heating to 375 °C + 30' show that Al and Al_3Ni are still present. Moreover, in the Cu-free alloy the stable phase is now fully developed. The nearness of the fourth DSC reaction in the Cu-free alloy, indeed starting before the third one finishes, makes it to easily take place during the isothermal treating, being the cause for the transformation of the metastable phase.

According to previous studies, the exact nature of the phases appearing after the third DSC reaction is uncertain. Thus, unknown phases are reported even after the end of the whole crystallisation process [16], or together to $\text{Al}_{11}\text{Sm}_3$ in $\text{Al}_{88}\text{-Sm}_8\text{-Ni}_4$ [17, 19]. Also, only binary phases such as Al_3Sm and Al_3Ni in $\text{Al}_{88}\text{-Sm}_4\text{-Ni}_8$ [18] (together to Al_4Sm and $\text{Al}_{11}\text{Sm}_3$ in $\text{Al}_{89}\text{-Sm}_5\text{-Ni}_6$ [23]), or a mixture of binary and ternary phases such as $\text{Al}_{11}\text{Sm}_3$ and Al_7SmNi_2 in $\text{Al}_{87}\text{-Sm}_6\text{-Ni}_7$ [14, 21, 22] are reported. This latter ternary phase is proposed because of its similarity with the XRD pattern in an Al-Nd-Ni alloy [30]. A newer and detailed study on high temperature crystallisation of Al-Sm-Ni systems [13] suggests the continuity of orthorhombic $\text{Al}_{11}\text{Sm}_3$ (with similar XRD peaks position as the metastable phase of this work) after the third DSC reaction, and the appearance of two new intermetallics, spherical tetragonal $\text{Al}_{11}\text{Sm}_3$ and elongated $\text{Al}_{23}\text{Sm}_4\text{Ni}_6$ (the latter a phase referred in the in the Al-Sm-Ni phase diagram [31], with similar XRD peaks position as the stable phase of this work). The fourth DSC reaction is related in [13] to the transformation of orthorhombic $\text{Al}_{11}\text{Sm}_3$ to orthorhombic Al_4Sm , and also in [32] to the reaction of the ternary and Al_3Ni phases, leading to the crystallisation of Al_9YNi_3 in Al-Y-Ni systems, or even to morphological changes in the phases. There are not enough evidences in this work to corroborate any of these particular transformations.

According to the XRD peak positions of this work, the metastable phase cannot be identified, and the stable phase could be highly probable identified as $\text{Al}_{19}\text{Sm}_3\text{Ni}_5$. To our knowledge, $\text{Al}_{19}\text{Sm}_3\text{Ni}_5$ has not been reported before in Al-Sm-Ni systems, but the similarity with $\text{Al}_{19}\text{Y}_3\text{Ni}_5$ in XRD peak positions and intensities, as reported in [32], ratify this possibility. According to the similitude between the lattice parameters of other known phases of these systems such as $\text{Al}_{23}\text{Sm}_4\text{Ni}_6$ and $\text{Al}_{23}\text{Y}_4\text{Ni}_6$ (1.5939, 0.40967, 1.8320 nm and 113.09° for the Sm compound [31], and 1.5836, 0.4068, 1.8311 nm and 112.97° for the Y compound [33]), this seems an acceptable hypothesis.

On the other hand, Cu-containing alloys do not change the previously observed pattern after treating the ribbons to 375 °C + 30'. Only after heating to 450 °C, peaks of $\text{Al}_{19}\text{Sm}_3\text{Ni}_5$ appear together with those of the metastable phase, and the total transformation to $\text{Al}_{19}\text{Sm}_3\text{Ni}_5$ is detected after heating to 600 °C. According to DSC traces shown in Figure 2, the transformation to the stable phase takes place in a wider range of temperatures from about 450 °C.

Figure 8 shows experimental and simulated (with PowderCell software [34]) patterns of Cu-containing alloys after being heat treated to 600 °C, considering a mixture of Al, $\text{Al}_{19}\text{Sm}_3\text{Ni}_5$ and Al_3Ni . Despite the proportions considered for each phase are rough figures and only a qualitative comparison can be carried out, the low presence of Al_3Ni does not affect the simulation, and it could therefore intervene in the formation of the $\text{Al}_{19}\text{Sm}_3\text{Ni}_5$ phase. The crystalline structure and atomic positions for the $\text{Al}_{19}\text{Sm}_3\text{Ni}_5$ have been taken from the $\text{Al}_{19}\text{Y}_3\text{Ni}_5$ phase (space group *Cmcm*, Pearson symbol *oC108* and lattice parameters 0.403, 1.598 and 2.689 nm [35]), and only a small change of the lattice parameters to 0.410, 1.598 and 2.689 nm has been necessary for a better simulation coincident with the experimental pattern.

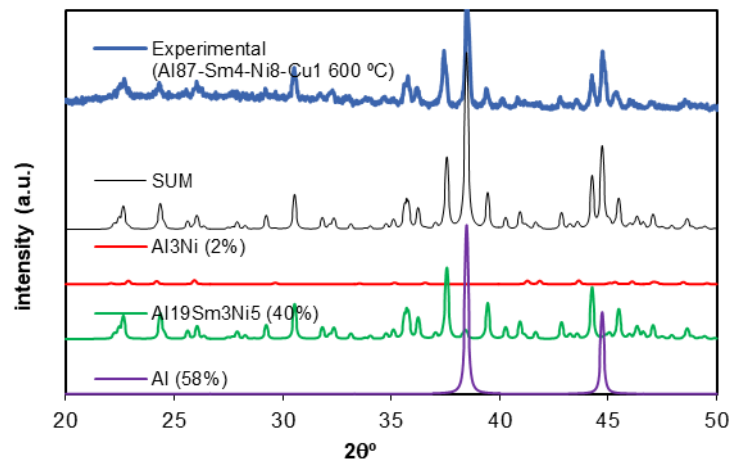


Figure 8. Experimental and simulated XRD patterns of $\text{Al}_{87}\text{-Sm}_4\text{-Ni}_8\text{-Cu}_1$ alloy heat treated to 600 °C. The simulation considers of Al, $\text{Al}_{19}\text{Sm}_3\text{Ni}_5$, and Al_3Ni in proportions 58/40/2.

In summary, Al and Al_3Ni are present after the high temperature heat treatments, with Al appearing in the first and Al_3Ni during the second DSC reaction. The second reaction also causes the formation of the first Al-Sm-Ni intermetallic, as an unidentified metastable phase. Furthermore, this ternary phase grows during the third DSC reaction, and there is a subsequent evolution from the metastable phase to the stable $\text{Al}_{19}\text{Sm}_3\text{Ni}_5$. A detailed examination of particular intermetallic grains could help confirming this microstructural evolution.

3.6. Microstructural identification

Phases identification, and size and shape evolution, have been carried out by TEM microdiffraction on specific particles. For the alloys and heat treatments studied, Al and Al_3Ni identified particles always had an equiaxial shape. During the next discussion these two phases will not be considered.

Figure 9 shows the microstructure of the three studied alloys after heating to 375 °C + 30'. Apart from equiaxial phases, elongated particles with a maximum of approximately 500 nm are observed.

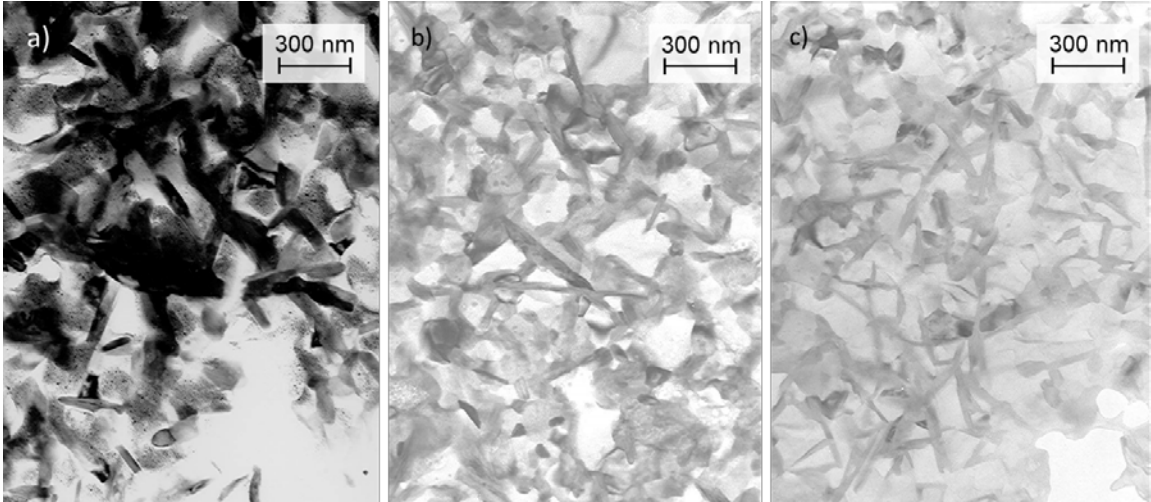


Figure 9. TEM bright field images of ribbons heat treated to 375 °C + 30' of a) $\text{Al}_{88}\text{-Sm}_4\text{-Ni}_8$, b) $\text{Al}_{87}\text{-Sm}_4\text{-Ni}_8\text{-Cu}_1$ and c) $\text{Al}_{88}\text{-Sm}_4\text{-Ni}_7\text{-Cu}_1$ alloys.

In the Cu-free alloy, in which the $\text{Al}_{19}\text{Sm}_3\text{Ni}_5$ phase has already appeared from the metastable phase, the intermetallics tend to appear with rod shape, although relatively equiaxial shapes cannot be discarded for this phase. On the contrary, intermetallics seem to appear with acicular shapes in Cu-containing alloys, in which the metastable phase is still the only phase present at 375 °C + 30'.

The microstructure of these alloys after heating to 450 °C is shown in Figure 10, being similar to that obtained at 600 °C. The main visible change with respect to 375 °C + 30' is the size of the different phases, mainly in the acicular phase of Cu-containing alloys, in general now above 500 nm long.

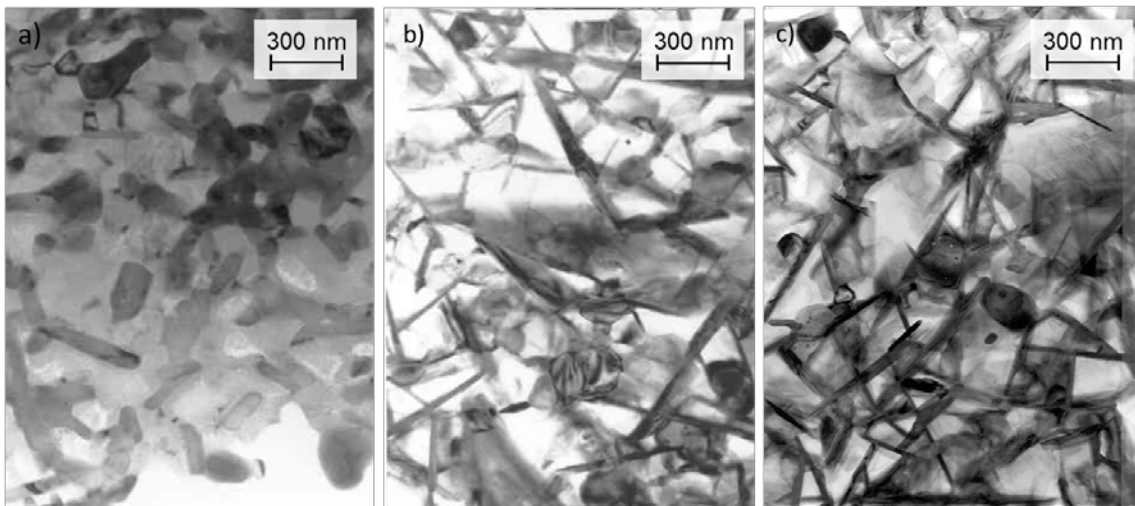


Figure 10. TEM bright field images of ribbons heat treated to 450 °C of a) $\text{Al}_{88}\text{-Sm}_4\text{-Ni}_8$, b) $\text{Al}_{87}\text{-Sm}_4\text{-Ni}_8\text{-Cu}_1$ and c) $\text{Al}_{88}\text{-Sm}_4\text{-Ni}_7\text{-Cu}_1$ alloys.

Comparing particles shape for different temperatures, and considering at the same time the XRD results, it can be confirmed that, for the Cu-free alloy, the quick transformation to $\text{Al}_{19}\text{Sm}_3\text{Ni}_5$ makes this phase to maintain the rod shapes that the metastable phase had only reached, although equiaxial shapes could also be present. On the other hand, for Cu-containing alloys, the metastable phase had time enough to reach much more elongated shapes, and when part (after 450 °C) or the total (at 600 °C) of the metastable phase disappears, leading to $\text{Al}_{19}\text{Sm}_3\text{Ni}_5$, the acicular shape that the metastable phase had developed seems to be the shape found in the microstructure. It is possible therefore to suggest that the transformation from the metastable phase to $\text{Al}_{19}\text{Sm}_3\text{Ni}_5$ takes place without change in particles shape. Accordingly, both phases probably have a very similar crystalline structure and chemical composition, not needing a new nucleation process.

The study of these particles with TEM microdiffraction (Figure 11) shows that at 450 °C, in the Cu-free alloy, the phase $\text{Al}_{19}\text{Sm}_3\text{Ni}_5$ is effectively found with both rounded and rod shapes, although the occurrence of the rod shape is much more observed. As expected, for the Cu-containing alloys at 450 °C, $\text{Al}_{19}\text{Sm}_3\text{Ni}_5$ is only identified with acicular shape.

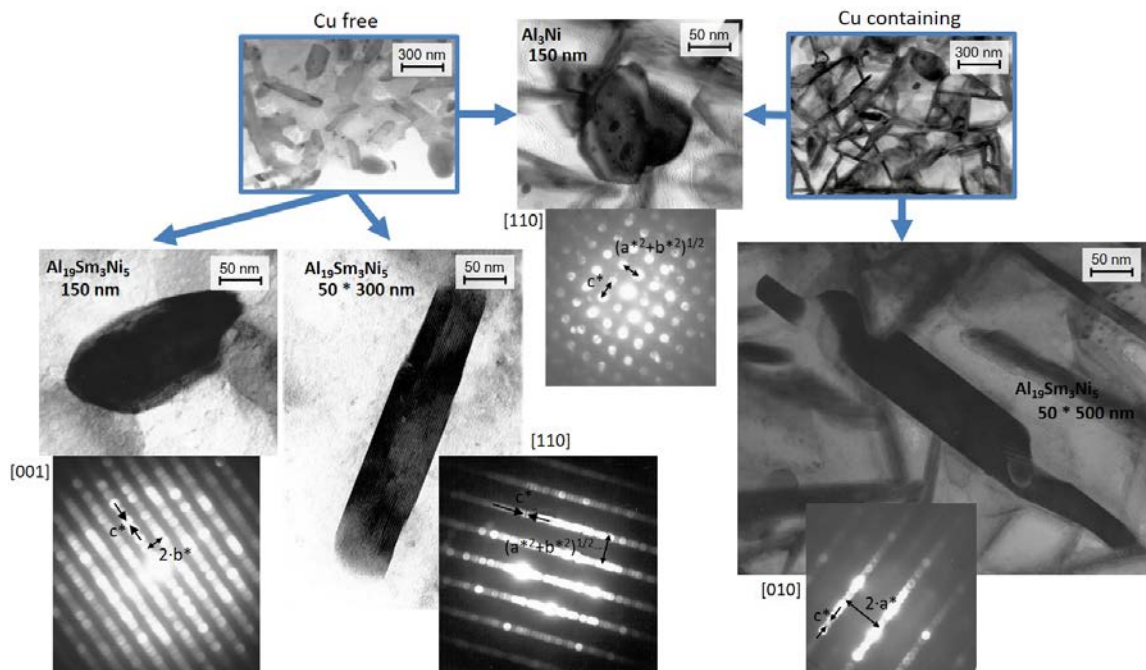


Figure 11. TEM bright field micrographs and selected particles microdiffraction patterns of heat treated ribbons up to 450 °C. Reciprocal lattice parameters are indicated in the DP.

As previously made for XRD, the identification of the $\text{Al}_{19}\text{Sm}_3\text{Ni}_5$ phase in the DP has been carried out by considering slightly changed lattice parameters (0.410, 1.598 and 2.689 nm) to those known for the orthorhombic $\text{Al}_{19}\text{Y}_3\text{Ni}_5$.

Finally, Figure 12 shows the TEM microdiffraction study of an intermetallic particle of the $\text{Al}_{87}\text{-Sm}_4\text{-Ni}_8\text{-Cu}_1$ alloy after heat treating the ribbon to 375 °C + 30', where only the metastable phase is present.

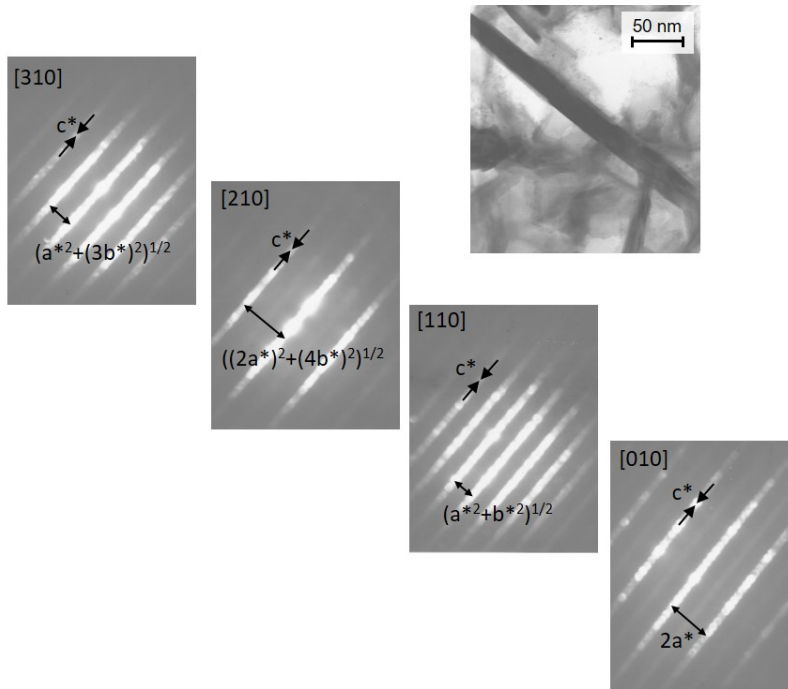


Figure 12. Study of an intermetallic particle of the $\text{Al}_{87}\text{-Sm}_4\text{-Ni}_8\text{-Cu}_1$ alloy heated to 375 °C + 30'. Diffraction patterns are identified according to the angles between the four patterns and approximated diffraction spots distances.

Measurements of spot distances on the four DP of Figure 12 allow refining the reciprocal lattice of the metastable intermetallic. Once transformed to real lattice parameters, result in values of about 0.406, 1.864 and 2.805 nm, indeed quite similar to those previously considered for the $\text{Al}_{19}\text{Sm}_3\text{Ni}_5$ phase (0.410, 1.598 and 2.689 nm). It is therefore confirmed the probable similarity between the metastable and the stable $\text{Al}_{19}\text{Sm}_3\text{Ni}_5$ phases.

The previous lattice parameter values are a simple approximation based on direct measurements on TEM images, and depending, among other factors, on the precise calibration of the TEM camera length. However, considering the same atomic distribution that in the $\text{Al}_{19}\text{Sm}_3\text{Ni}_5$ or $\text{Al}_{19}\text{Y}_3\text{Ni}_5$ phase, the XRD pattern of the $\text{Al}_{87}\text{-Sm}_4\text{-Ni}_8\text{-Cu}_1$ alloy after heat treating the ribbon to $375\text{ }^\circ\text{C} + 30'$ has been simulated and presented in Figure 13. The experimental pattern is also shown. As observed, the simulated pattern is very similar to the experimental one.

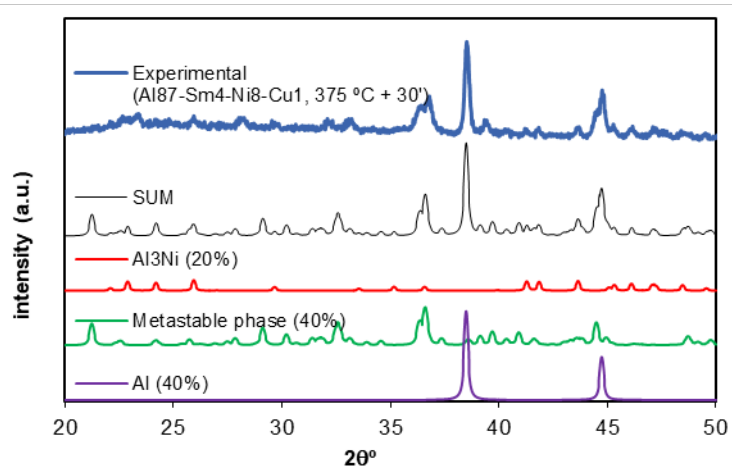


Figure 13. Experimental and simulated XRD patterns of the $\text{Al}_{87}\text{-Sm}_4\text{-Ni}_8\text{-Cu}_1$ alloy after heat treating the ribbon to $375\text{ }^\circ\text{C} + 30'$. The simulated pattern considers the presence of Al, Al_3Ni , and the metastable phase in proportions 40/40/20.

Despite the description of microstructural evolution and phases identification, there is still an important detail to clarify, the precise effect of Cu. STEM studies were carried out to clarify the distribution of Cu in the microstructure of the $\text{Al}_{87}\text{-Sm}_4\text{-Ni}_8\text{-Cu}_1$ alloy after heat treating the ribbon to $375\text{ }^\circ\text{C} + 30'$ (Figure 14).

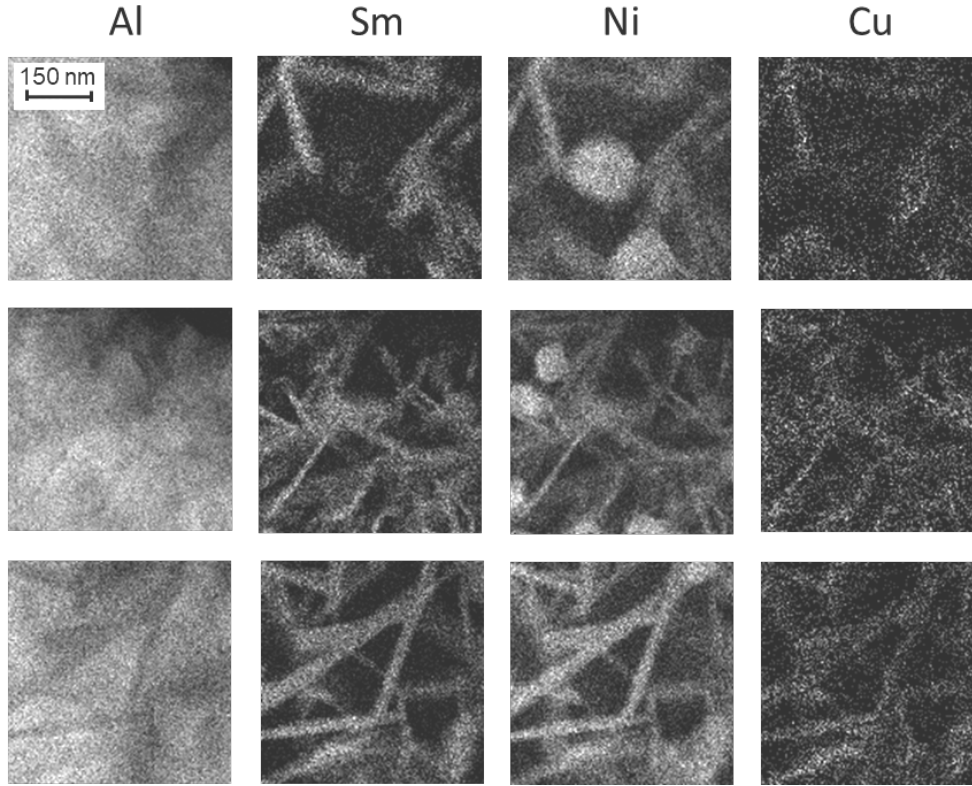


Figure 14. STEM EDX maps from different areas of an $\text{Al}_{88}\text{-Sm}_4\text{-Ni}_7\text{-Cu}_1$ alloy heated to $375\text{ }^\circ\text{C} + 30'$.

As can be seen, an Al background is found in the different areas studied. Also rounded shapes of Al_3Ni appear free of Sm. Elongated intermetallics, as expected, contain Al, Sm and Ni, with Cu found to be preferentially in this metastable Al-Sm-Ni phase.

Nevertheless, even with the STEM and the simulation results in mind, further work is necessary to precisely define the nature and crystalline structure both of the possible $\text{Al}_{19}\text{Sm}_3\text{Ni}_5$ phase, and mainly of the metastable phase.

4. Conclusions.

Adding 1 at.% Cu to the $\text{Al}_{88}\text{-Sm}_4\text{-Ni}_8$ alloy changes the thermal stability of the obtained amorphous melt-spun material. If Cu substitutes Al, the stability of the amorphous structure increases, whereas substituting Ni decreases the stability. In both cases, the presence of Cu results on the size reduction of the primary $\alpha\text{-Al}$ nanocrystals.

Differences because of the presence of Cu again appear at higher temperatures, during crystallisation of Al, Al₃Ni, and ternary Al-Sm-Ni intermetallics. The ternary phase appears with a metastable structure. The presence of Cu increases the prevalence of the metastable phase. Al₁₉Sm₃Ni₅ phase is proposed as the probable stable ternary phase because of its similitude with Al-Y-Ni alloys.

The metastable phase tends to develop an elongated acicular shape. In the Cu-free alloy, in which the Al₁₉Sm₃Ni₅ quickly appears, the elongated shape is restricted and rod shapes predominate. Once the metastable phase transforms to Al₁₉Sm₃Ni₅ at higher temperatures, without new nucleation process, the stable phase appears with the previous shape of the metastable phase, i.e., acicular shape for Cu-containing alloys.

Therefore, Cu addition affects the primary crystallisation of α -Al, with smaller nanocrystals being formed. However, after the later stages of crystallisation, the appearance of elongated intermetallics in Cu-containing alloys will surely affect mechanical behaviour.

Acknowledgements

The Ministerio de Economía y Competitividad (Spain) and Feder (EU) through the research project DPI2015-69550-C2-2-P are gratefully acknowledged for financial support. The authors also wish to thank Prof. Brian Cantor and Dr. Paul J. Warren for helpful discussion and facilitating the initial experiments carried out at Materials Department of Oxford University.

Declarations of interest: none

References

- [1] J. Yin, H. Cai, X. Cheng, X. Zhang, Al-based bulk metallic glass with large plasticity and ultrahigh strength, *Journal of Alloys and Compounds* 648 (2015), 276-279.
- [2] Y.H. Kim, A. Inoue, T. Masumoto, Ultrahigh Mechanical Strengths of Al₈₈Y₂Ni₁₀-xM_x (M=Mn, Fe or Co) Amorphous Alloys Containing Nanoscale fcc-Al Particles, *Mater. Trans., JIM* 32 (1991), 599-608.

- [3] Y.H. Kim, A. Inoue, T. Matsumoto, Ultrahigh tensile strengths of Al₈₈Y₂Ni₉M₁ (M=Mn or Fe) amorphous alloys containing finely dispersed fcc-Al particles, *Mater. Trans., JIM*. 31 (1990), 747-749.
- [4] Y.H. Kim, A. Inoue, T. Matsumoto, Increase in Mechanical Strength of Al–Y–Ni Amorphous Alloys by Dispersion of Nanoscale fcc-Al Particles, *Mater. Trans., JIM*. 32 (1991), 331-338.
- [5] Z.C. Zhong, X.Y. Jiang, A.L. Greer, Micro structure and hardening of Al-based nanophase composites, *Mater. Sci. Eng. A* 226–228 (1997), 531-535.
- [6] H.S. Kim, P.J. Warren, B. Cantor, H.R. Lee, Mechanical properties of partially crystallized aluminium based amorphous alloys, *NanoStructured Materials* 11(2) (1999), 241-247.
- [7] Y. Zhang, P.J. Warren, A. Cerezo. Effect of Cu addition on nanocrystallization of Al-Ni-Sm amorphous alloy, *Materials Science & Engineering A* 327 (2002) 109-115.
- [8] L. Battezzati, M. Baricco, P. Schumacher, W.C. Shih, A.L. Greer, Crystallization behaviour of Al-Sm amorphous alloys, *Mater. Sci. & Eng. A* 179-180 (1994) 600-604.
- [9] R.S. Maurya, A. Sahu, T. Laha, Quantitative phase analysis in Al₈₆Ni₈Y₆ bulk glassy alloy synthesized by consolidating mechanically alloyed amorphous powder via spark plasma sintering, *Materials and Design* 93 (2016), 96-103.
- [10] R.S. Maurya, A. Sahu, T. Laha, Effect of consolidation pressure on phase evolution during sintering of mechanically alloyed Al₈₆Ni₈Y₆ amorphous powders via spark plasma sintering, *Materials Science and Engineering A* 649 (2016), 48-56.
- [11] C. Chattopadhyay, B.S. Murty, Kinetic modification of the ‘confusion principle’ for metallic glass formation, *Scripta Materialia* 116 (2016), 7-10.
- [12] V. Sidorov, P. Svec, P. Svec Sr., D. Janickovic, V. Mikhailov, E. Sidorova, L. Son, Electric and magnetic properties of Al₈₆Ni₈R₆ (R=Sm, Gd, Ho) alloys in liquid and amorphous states, *Journal of Magnetism and Magnetic Materials* 408 (2016) 35-40.
- [13] A. Anghelus, M-N. Avettand-Fènoël, C. Cordier, R. Taillard, Thermal crystallization of an Al₈₈Ni₆Sm₆ metallic glass, *Journal of Alloys and Compounds* 651 (2015) 454-464.
- [14] L. Battezzati, M. Kusy, P. Rizzi, V. Ronto, Devitrification of Al-Ni-Rare Earth amorphous alloys, *Journal of Materials Science* 39 (2004) 3927-3934.
- [15] S.A. Uporov, R.E. Ryl'tsev, N.S. Uporova, V.A. Bykov, A.M. Murzakaev, S.V. Pryanichnikov, Structural and Magnetic Peculiarities of

Al₈₆Ni₈Sm₆ Alloy in Amorphous, Crystalline, and Liquid States, *The Physics of Metals and Metallography* 116(2) (2015) 128-135.

[16] T. Gloriant, A.L. Greer, Al-Based nanocrystalline composites by rapid solidification of Al-Ni-Sm alloys, *NanoStructured Materials*. 10(3) (1998) 389-396.

[17] M. Gich, T. Gloriant, S. Suriñach, A.L. Greer, M.D. Baró, Glass forming ability and crystallisation processes within the Al-Ni-Sm system, *Journal of Non-Crystalline Solids* 289 (2001) 214-220.

[18] Á. Révész, L.K. Varga, P.M. Nagy, J. Lendvai, I. Bakonyi, Structure and thermal stability of melt-quenched Al_{92-x}Ni₈(Ce,Sm)_x alloys with x=1, 2 and 4, *Materials Science and Engineering A* 351 (2003) 160-165.

[19] F. Sun, T. Gloriant, Primary crystallization process of amorphous Al₈₈Ni₆Sm₆ alloy investigated by differential scanning calorimetry and by electrical resistivity, *Journal of Alloys and Compounds* 477 (2009) 133-138.

[20] A. Anghelus, M-N. Avettand-Fènoël, C. Cordier, R. Taillard, Microstructural evolution of aluminium/Al-Ni-Sm glass forming alloy laminates obtained by Controlled Accumulative Roll Bonding, *Journal of Alloys and Compounds* 631 (2015) 209-218.

[21] L. Battezzati, P. Rizzi, V. Rontó, The difference in devitrification paths in Al₈₇Ni₇Sm₆ and Al₈₇Ni₇La₆ amorphous alloys, *Materials Science and Engineering A* 375-377 (2004) 927-931.

[22] V. Rontó, L. Battezzati, A.R. Yavari, M. Tonegaru, N. Lupu, G. Heunen, Crystallization behaviour of Al₈₇Ni₇La₆ and Al₈₇Ni₇Sm₆ amorphous alloys, *Scripta Materialia* 50 (2004) 839-843.

[23] E. Illeková, P. Duhaj, P. Mrafko, P. Svec, Influence of Pd on crystallization of Al-Ni-Sm-based ribbons, *Journal of Alloys and Compounds* 483 (2009) 20-23

[24] T. Gloriant, D.H. Ping, K. Hono, A.L. Greer, M.D. Baró, Nanostructured Al₈₈Ni₄Sm₈ alloys investigated by transmission electron and field-ion microscopies, *Materials Science and Engineering A* 304-306 (2001) 315-320.

[25] J. Latuch, H. Matyja, V.I. Fadeeva, Crystallization of amorphous Al₈₅Y₁₀Ni₅ and Al₈₅Y₅Ni₁₀ alloys, *Materials Science and Engineering, A* 179-180 (1994), 506-510.

[26] Z.H. Huang, J.F. Li, Q.L. Rao, Y.H. Zhou, Primary crystallization of Al-Ni-RE amorphous alloys with different type and content of RE, *Materials Science and Engineering A* 489(1-2) (2008), 380-388.

[27] S.J. Hong, P.J. Warren, B.S. Chun, Nanocrystallization behaviour of Al-Y-Ni with Cu additions, *Materials Science and Engineering A* 304-306 (2001) 362-366.

- [28] K. Hono, Y. Zhang, A. Inoue, T. Sakurai, Atom Probe Studies of Nanocrystalline Microstructural Evolution in Some Amorphous Alloys, *Mater. Trans.*, JIM 36 (1995), 909-917.
- [29] M. Matsuura, M. Sakurai, K. Suzuki, A.P. Tsai, A. Inoue, Local structure change of Ce and Cu in the course of nanocrystalline formation from amorphous Al₈₇Ni₈Ce₃Cu₂, *Materials Science and Engineering A* 226-228 (1997) 511-514.
- [30] L. Battezzati, S. Pozzovivo, P. Rizzi, Phase Transformations in Al₈₇Ni₇Ce₆ and Al₈₇Ni₇Nd₆ amorphous alloys, *Mater. Trans.* 43 (2002) 2593-2599.
- [31] S. Delsante, R. Raggio, G. Borzone, Phase relations of the Sm–Ni–Al ternary system at 500 °C in the 40–100 at.% Al region, *Intermetallics* 16 (2008) 1250-1257.
- [32] M.D.H. Lay, A.J. Hill, P.G. Saksida, M.A. Gibson, T.J. Bastow, ²⁷Al NMR measurement of fcc Al configurations in as-quenched Al₈₅Ni₁₁Y₄ metallic glass and crystallization kinetics of Al nanocrystals, *Acta Materialia* 60(1) (2012), 79-88.
- [33] R. Raggio, G. Borzone, Riccardo Ferro, The Al-rich region in the Y–Ni–Al system: microstructures and phase equilibria, *Intermetallics* 8 (2000), 247-257.
- [34] G. Nolze, W. Klaus, PowderCell 2.0 for Windows, *Powder Diffraction* 13(4) (1998) 256-259.
- [35] D. Shin, W.J. Golumbskie, E.R. Ryba, Z.-K. Liu, First-principles study of Al–Ni–Y ternary compounds for crystal structure validation, *J Alloys Comp* 462 (2008) 262-266.